NON-MARKOVIAN THEORY OF VIBRATIONAL ENERGY RELAXATION AND ITS APPLICATIONS TO BIOMOLECULAR SYSTEMS

HIROSHI FUJISAKI,[1,2] YONG ZHANG,[3] and JOHN E. STRAUB[4]

[1]*Molecular Scale Team, Integrated Simulation of Living Matter Group, Computational Science Research Program, RIKEN, 2-1 Hirosawa, Wako-shi, Saitama 351-0198, Japan*
[2]*Department of Physics, Nippon Medical School 2-297-2 Kosugi-cho, Nakahara, Kawasaki, Kanagawa 211-0063, Japan*
[3]*Department of Chemical and Biomolecular Engineering, University of Notre Dame, 182 Fitzpatrick Hall, Notre Dame, IN 46556-5637, USA*
[4]*Department of Chemistry, Boston University, 590 Commonwealth Avenue, SCI 503, Boston, MA 02215, USA*

CONTENTS

Advancing Theory for Kinetics and Dynamics of Complex, Many-Dimensional Systems: Clusters and Proteins, Advances in Chemical Physics, Volume 145, Edited by Tamiki Komatsuzaki, R. Stephen Berry, and David M. Leitner.

I. INTRODUCTION

Energy transfer (relaxation) phenomena are ubiquitous in nature. At a macroscopic level, the phenomenological theory of heat (Fourier law) successfully describes heat transfer and energy flow. However, its microscopic origin is still under debate. This is because the phenomena can contain many-body, multiscale, nonequilibrium, and even quantum mechanical aspects, which present significant challenges to theories addressing energy transfer phenomena in physics, chemistry, and biology [1]. For example, heat generation and transfer in nanodevices is a critical problem in the design of nanotechnology. In molecular physics, it is well known that vibrational energy relaxation (VER) is an essential aspect of any quantitative description of chemical reactions [2]. In the celebrated RRKM theory of an absolute reaction rate for isolated molecules, it is assumed that the intramolecular vibrational energy relaxation (IVR) is much faster than the reaction itself. Under certain statistical assumptions, the reaction rate can be derived [3]. For chemical reactions in solutions, the transition state theory and its extension such as Kramer's theory and the Grote–Hynes theory have been developed [4, 5] and applied to a variety of chemical systems including biomolecular systems [6]. However, one cannot always assume separation of timescales. It has been shown that a conformational transition (or reaction) rate can be modulated by the IVR rate [7]. As this brief survey demonstrates, a detailed understanding of IVR or VER is essential to study the chemical reaction and conformation change of molecules.

A relatively well-understood class of VER is a single vibrational mode embedded in (vibrational) bath modes. If the coupling between the system and the bath modes is weak (or assumed to be weak), a Fermi's-golden-rule style formula derived using second-order perturbation theory [8–10] may be used to estimate the VER rate. However, the application of such theories to real molecular systems poses several (technical) challenges, including how to choose force fields, how to separate quantum and classical degrees of freedom, or how to treat the separation of timescales between system and bath modes. Multiple solutions have been proposed to meet those challenges leading to a variety of theoretical approaches to the treatment of VER [11–16]. These works using Fermi's golden rule are based on quantum mechanics and are suitable for the description of high-frequency modes (more than thermal energy $\simeq$200 cm^{-1}), on which nonlinear spectroscopy has recently focused [17–20].

In this chapter, we summarize our recent work on VER of high-frequency modes in biomolecular systems. In our previous work, we have concentrated on the VER rate and mechanisms for proteins [21]. Here we shall focus on the time course of the VER dynamics. We extend our previous Markovian theory of VER to a non-Markovian theory applicable to a broader range of chemical systems [22, 23]. Recent time-resolved spectroscopy can detect the time course of VER dynamics (with femtosecond resolution), which may not be accurately described by a single

timescale. We derive new formulas for VER dynamics and apply them to several interesting cases, where comparison to experimental data is available.

This chapter is organized as follows: In Section II, we briefly summarize the normal mode concepts in protein dynamics simulations, on which we build our non-Markovian VER theory. In Section III, we derive VER formulas under several assumptions and discuss the limitations of our formulas. In Section IV, we apply the VER formulas to several situations: the amide I modes in isolated and solvated *N*-methylacetamide and cytochrome *c*, and two in-plane modes (ν_4 and ν_7 modes) in a porphyrin ligated to imidazole. We employ a number of approximations in describing the potential energy surface (PES) on which the dynamics takes place, including the empirical CHARMM [24] force-field and density functional calculations [25] for the small parts of the system (*N*-methylacetamide and porphyrin). We compare our theoretical results with experiment when available, and find good agreement. We can deduce the VER mechanism based on our theory for each case. In Section V, we summarize and discuss the further aspects of VER in biomolecules and in nanotechnology (molecular devices).

II. NORMAL MODE CONCEPTS APPLIED TO PROTEIN DYNAMICS

Normal mode provides a powerful tool in exploring molecular vibrational dynamics [26] and may be applied to biomolecules as well [27]. The first normal mode calculations for a protein were performed for BPTI protein [28]. Most biomolecular simulation softwares support the calculation of normal modes [24, 29, 30]. However, the calculation of a mass-weighted Hessian K_{ij}, which requires the second derivatives of the potential energy surface, with elements defined as

$$K_{ij} = \frac{1}{\sqrt{m_i m_j}} \frac{\partial^2 V}{\partial x_i \partial x_j} \tag{1}$$

can be computationally demanding. Here m_i is the mass, x_i is the coordinate, and V is the potential energy of the system. Efficient methods have been devised including torsional angle normal mode [31], block normal mode [32], and the iterative mixed-basis diagonalization (DIMB) methods [33], among others. An alternative direction for efficient calculation of a Hessian is to use coarse-grained models such as elastic [34] or Gaussian network [35] models. From normal mode analysis (or instantaneous normal mode analysis [36]), the frequencies, the density of states, and the normal mode vectors can be calculated. In particular, the last quantity is important because it is known that the lowest eigenvectors may describe the functionally important motions such as large-scale conformational change, a subject that is the focus of another chapter of this volume [37].

There is no doubt as to the usefulness of normal mode concepts. However, for molecular systems, it is always an approximate model as higher order nonlinear

coupling and intrinsic anharmonicity become essential. To describe energy transfer (or relaxation) phenomena in a protein, Moritsugu, Miyashita, and Kidera (MMK) introduced a reduced model using normal modes with third- and fourth-order anharmonicity [38], $C^{(3)}_{klm}$ and $C^{(4)}_{klmn}$, respectively,

$$V(\{q_k\}) = \sum_k \frac{\omega_k^2}{2} q_k^2 + \frac{1}{3!} \sum_{klm} C^{(3)}_{klm} q_k q_l q_m + \frac{1}{4!} \sum_{klmn} C^{(4)}_{klmn} q_k q_l q_m q_n \qquad (2)$$

with

$$C^{(3)}_{klm} \equiv \frac{\partial^3 V}{\partial q_k \partial q_l \partial q_m} \qquad (3)$$

$$C^{(4)}_{klmn} \equiv \frac{\partial^4 V}{\partial q_k \partial q_l \partial q_m \partial q_n} \qquad (4)$$

where q_k denotes the normal mode calculated by the Hessian K_{ij} and ω_k is the normal mode frequency. Classical (and harmonic) Fermi resonance [39] is a key ingredient in the MMK theory of energy transfer derived from observations of all-atom simulations of myoglobin at zero temperature (see Fig. 1).

At finite temperature, nonresonant effects become important and clear interpretation of the numerical results becomes difficult within the classical approximation. Nagaoka and coworkers [40] identified essential vibrational modes in vacuum simulations of myoglobin and connected these modes to the mechanism of "heme cooling" explored experimentally by Mizutani and Kitagawa [18]. Contemporaneously, nonequilibrium MD simulations of solvated myoglobin carried out by Sagnella and Straub provided the first detailed and accurate simulation of heme cooling dynamics [41]. That work supported the conjecture that the motion

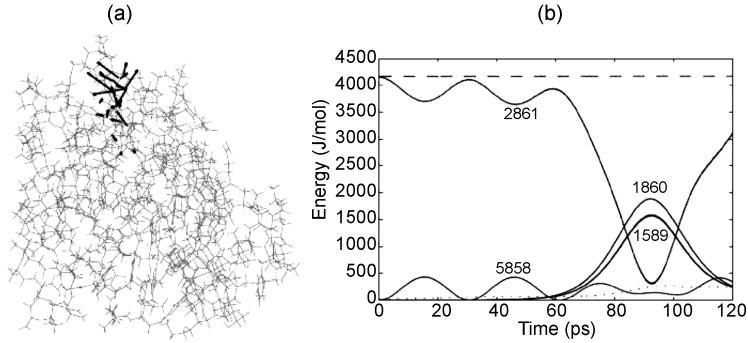

Figure 1. (**a**) The excited eigenvector depicted by arrows in myoglobin. (**b**) Classical simulation of mode-specific energy transfer in myoglobin at zero temperature. (Reproduced with permission from Ref. 38. Copyright 2009 by the American Physical Society.)

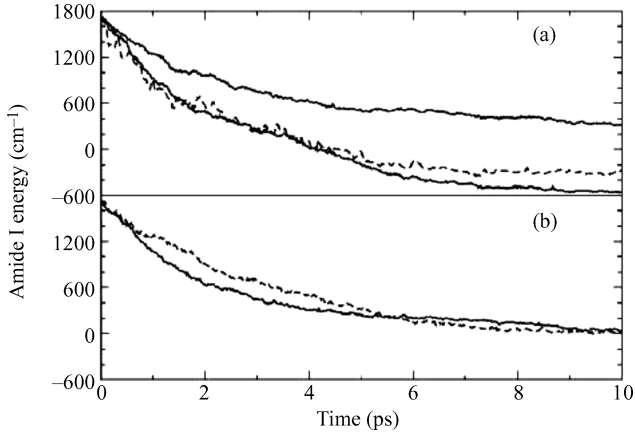

Figure 2. Nonequilibrium MD simulation of energy flow from the excited amide I mode in *N*-methylacetamide in heavy water. See also Fig. 3. (Reproduced with permission from Ref. 42. Copyright 2009 by the American Institute of Physics.)

similar to those modes identified by Nagaoka plays an important role in energy flow pathways.

Nguyen and Stock explored the vibrational dynamics of the small molecule, *N*-methylacetamide (NMA) often used as a model of the peptide backbone [42]. Using nonequilibrium MD simulations of NMA in heavy water, VER was observed to occur on a picosecond timescale for the amide I vibrational mode (see Fig. 2). They used the instantaneous normal mode concept [36] to interpret their result and noted the essential role of anharmonic coupling. Leitner also used the normal mode concept to describe energy diffusion in a protein and found an interesting link between the anomalous heat diffusion and the geometrical properties of a protein [43].

In terms of vibrational spectroscopy, Gerber and coworkers calculated the anharmonic frequencies in BPTI, within the VSCF level of theory [44], using the reduced model [Eq. (2)]. Yagi, et al. refined this type of anharmonic frequency calculation for large molecular systems with more efficient methods [45], appropriate for applications to biomolecules such as DNA base pair [46]. Based on the reduced model [Eq. (2)] with higher order nonlinear coupling, Leitner also studied quantum mechanical aspects of VER in proteins, by employing the Maradudin–Fein theory based on Fermi's golden rule [12]. Using the same model, Fujisaki, Zhang, and Straub focused on more detailed aspects of VER in biomolecular systems and calculated the VER rate, mechanisms, or pathways, using their non-Markovian perturbative formulas (described in Section III).

As this brief survey demonstrates, the normal mode concept is a powerful tool that provides significant insight into mode-specific vibrational dynamics and energy transfer in proteins, when anharmonicity of the potential energy surface is taken into account.

III. DERIVATION OF NON-MARKOVIAN VER FORMULAS

We have derived a VER formula for the simplest situation, a one-dimensional relaxing oscillator coupled to a "static" bath [22]. Here we extend this treatment to two more general directions: (a) multidimensional relaxing modes coupled to a "static" bath and (b) a one-dimensional relaxing mode coupled to a "fluctuating" bath [47].

A. Multidimensional Relaxing Mode Coupled to a Static Bath

We take the following time-independent Hamiltonian:

$$\mathcal{H} = \mathcal{H}_S^0 + \mathcal{H}_B + \mathcal{V}^0 \tag{5}$$

$$= \mathcal{H}_S^0 + \langle \mathcal{V} \rangle_B + \mathcal{H}_B + \mathcal{V}^0 - \langle \mathcal{V} \rangle_B \tag{6}$$

$$= \mathcal{H}_S + \mathcal{H}_B + \mathcal{V} \tag{7}$$

where

$$\mathcal{H}_S \equiv \mathcal{H}_S^0 + \langle \mathcal{V} \rangle_B \tag{8}$$

$$\mathcal{V} \equiv \mathcal{V}^0 - \langle \mathcal{V} \rangle_B \tag{9}$$

In previous work [22], we have considered only a single one-dimensional oscillator as the system. Here we extend that treatment to the case of an N_S-dimensional oscillator system. That is,

$$\mathcal{H}_S = \sum_{i=1}^{N_S} \left(\frac{p_i^2}{2} + \frac{\omega_i^2}{2} q_i^2 \right) + V(\{q_i\}) \tag{10}$$

$$\mathcal{H}_B = \sum_{\alpha=1}^{N_B} \left(\frac{p_\alpha^2}{2} + \frac{\omega_\alpha^2}{2} q_\alpha^2 \right) \tag{11}$$

$$\mathcal{V} = -\sum_{i=1}^{N_S} q_i \delta \mathcal{F}_i(\{q_\alpha\}) \tag{12}$$

where $V(\{q_i\})$ is the interaction potential function between N_S system modes that can be described by, for example, the reduced model, Eq. (2). The simplest case

$V(\{q_i\}) = 0$ is trivial as each system mode may be treated separately within the perturbation approximation for $\mathcal{V}$.

We assume that $|k\rangle$ is a certain state in the Hilbert space spanned by $\mathcal{H}_S$. Then the reduced density matrix is

$$(\rho_S)_{mn}(t) = \langle m|e^{-i\mathcal{H}_S t/\hbar}\mathrm{Tr}_B\{\tilde{\rho}(t)\}e^{i\mathcal{H}_S t/\hbar}|n\rangle \tag{13}$$

where the tilde denotes the interaction picture. Substituting the time-dependent perturbation expansion

$$\begin{aligned}\tilde{\rho}(t) = \rho(0) &+ \frac{1}{i\hbar}\int_0^t dt'[\tilde{\mathcal{V}}(t'), \rho(0)] \\ &+ \frac{1}{(i\hbar)^2}\int_0^t dt' \int_0^{t'} dt''[\tilde{\mathcal{V}}(t'), [\tilde{\mathcal{V}}(t''), \rho(0)]] + \cdots\end{aligned} \tag{14}$$

into the above, we find

$$(\rho_S)_{mn}(t) \simeq (\rho_S)^{(0)}_{mn}(t) + (\rho_S)^{(1)}_{mn}(t) + (\rho_S)^{(2)}_{mn}(t) + \cdots \tag{15}$$

where

$$\begin{aligned}(\rho_S)^{(0)}_{mn}(t) &= \langle m|e^{-i\mathcal{H}_S t/\hbar}\rho_S(0)e^{i\mathcal{H}_S t/\hbar}|n\rangle, \\ &= \langle m(-t)|\rho_S(0)|n(-t)\rangle = \langle m|\rho_S(t)|n\rangle\end{aligned} \tag{16}$$

$$\begin{aligned}(\rho_S)^{(2)}_{mn}(t) &= \frac{1}{(i\hbar)^2}\int_0^t dt' \int_0^{t'} dt''\langle m|e^{-i\mathcal{H}_S t/\hbar}\mathrm{Tr}_B\{[\tilde{\mathcal{V}}(t'), [\tilde{\mathcal{V}}(t''), \rho(0)]]\}e^{i\mathcal{H}_S t/\hbar}|n\rangle \\ &= \frac{1}{(i\hbar)^2}\int_0^t dt' \int_0^{t'} dt'' \sum_{i,j}\langle m(-t)|[q_i(t')q_j(t'')\rho_S(0) \\ &\quad - q_j(t'')\rho_S(0)q_i(t')]|n(-t)\rangle\langle\delta\mathcal{F}_i(t')\delta\mathcal{F}_j(t'')\rangle_B \\ &\quad + \frac{1}{(i\hbar)^2}\int_0^t dt' \int_0^{t'} dt'' \sum_{i,j}\langle m(-t)|[\rho_S(0)q_j(t'')q_i(t') \\ &\quad - q_i(t')\rho_S(0)q_j(t'')]|n(-t)\rangle\langle\delta\mathcal{F}_j(t'')\delta\mathcal{F}_i(t')\rangle_B\end{aligned} \tag{17}$$

Here we have defined $|m(t)\rangle = e^{-i\mathcal{H}_S t/\hbar}|m\rangle$ and taken $(\rho_S)^{(1)}_{mn}(t) = 0$. Recognizing that we must evaluate expressions of the form

$$\begin{aligned}R_{mn;ij}(t; t', t'') &= \langle m(-t)|[q_i(t')q_j(t'')\rho_S(0)|n(-t)\rangle, \\ &\quad -\langle m(-t)|q_j(t'')\rho_S(0)q_i(t')]|n(-t)\rangle\end{aligned} \tag{18}$$

$$C_{ij}(t', t'') = \langle\delta\mathcal{F}_i(t')\delta\mathcal{F}_j(t'')\rangle_B \tag{19}$$

and their complex conjugates, $R^*_{nm;ij}(t;t',t'')$, $C^*_{ij}(t',t'')$, the second-order contribution can be written as

$$(\rho_S)^{(2)}_{mn}(t) = \frac{1}{(i\hbar)^2}\int_0^t dt' \int_0^{t'} dt'' \sum_{i,j}[R_{mn;ij}(t;t',t'')C_{ij}(t',t'') + R^*_{nm;ij}(t;t',t'')C^*_{ij}(t',t'')] \tag{20}$$

We can separately treat the two terms. Assuming that we can solve $\mathcal{H}_S|a\rangle = E_a|a\rangle$, we find

$$\begin{aligned} R_{mn;ij}(t;t',t'') = &\sum_{abcd}\langle m|a\rangle(q_i)_{ab}(q_j)_{bc}(\rho_S)_{cd}\langle d|n\rangle \\ &\times e^{-i(E_a-E_d)t-i(E_b-E_a)t'-i(E_c-E_b)t''} \\ &-\sum_{abcd}\langle m|a\rangle(q_j)_{ab}(\rho_S)_{bc}(q_i)_{cd}\langle d|n\rangle \\ &\times e^{-i(E_a-E_d)t-i(E_d-E_c)t'-i(E_b-E_a)t''} \end{aligned} \tag{21}$$

For the bath-averaged term, we assume the following force due to third-order nonlinear coupling of system mode i to the normal modes, α and β, of the bath [21]:

$$\delta\mathcal{F}_i(\{q_\alpha\}) = \sum_{\alpha,\beta} C_{i\alpha\beta}(q_\alpha q_\beta - \langle q_\alpha q_\beta\rangle) \tag{22}$$

and we have [21]

$$C_{ij}(t',t'') = R^{--}_{ij}(t',t'') + R^{++}_{ij}(t',t'') + R^{+-}_{ij}(t',t'') \tag{23}$$

with

$$R^{--}_{ij}(t',t'') = \frac{\hbar^2}{2}\sum_{\alpha,\beta} D_{\alpha\beta;ij}(1+n_\alpha)(1+n_\beta)e^{-i(\omega_\alpha+\omega_\beta)(t'-t'')} \tag{24}$$

$$R^{++}_{ij}(t',t'') = \frac{\hbar^2}{2}\sum_{\alpha,\beta} D_{\alpha\beta;ij}n_\alpha n_\beta e^{i(\omega_\alpha+\omega_\beta)(t'-t'')} \tag{25}$$

$$R^{+-}_{ij}(t',t'') = \hbar^2\sum_{\alpha,\beta} D_{\alpha\beta;ij}(1+n_\alpha)n_\beta e^{-i(\omega_\alpha-\omega_\beta)(t'-t'')} \tag{26}$$

where

$$D_{\alpha\beta;ij} = \frac{C_{i\alpha\beta}C_{j\alpha\beta}}{\omega_\alpha\omega_\beta} \tag{27}$$

and n_α is the thermal population of the bath mode α.

This formula reduces to our previous result for a one-dimensional system oscillator [22] when $N_S = 1$ and all indices (i, j) are suppressed. Importantly, this formula can be applied to situations where it is difficult to define a "good" normal mode to serve as a one-dimensional relaxing mode, as in the case of the CH stretching modes of a methyl group [21]. However, expanding to an N_S-dimensional system adds the burden of solving the multidimensional Schrödinger equation $\mathcal{H}_S|a\rangle = E_a|a\rangle$. To address this challenge, we may employ vibrational self-consistent field (VSCF) theory and its extensions developed by Bowman and coworkers [48] implemented in MULTIMODE program of Carter and Bowman [49] or in the SINDO program of Yagi and coworkers [50]. As in the case of our previous theory of a one-dimensional system mode, we must calculate N_S-tiple third-order coupling constants $C_{i\alpha\beta}(i = 1, 2, ..., N_S)$ for all bath modes α and β.

B. One-Dimensional Relaxing Mode Coupled to a Fluctuating Bath

We start from the following time-dependent Hamiltonian:

$$\mathcal{H}(t) = \mathcal{H}_S^0(t) + \mathcal{H}_B(t) + \mathcal{V}^0(t) \tag{28}$$

$$= \mathcal{H}_S^0(t) + \langle \mathcal{V}(t) \rangle_B + \mathcal{H}_B(t) + \mathcal{V}^0(t) - \langle \mathcal{V}(t) \rangle_B \tag{29}$$

$$= \mathcal{H}_S(t) + \mathcal{H}_B(t) + \mathcal{V}(t) \tag{30}$$

where

$$\mathcal{H}_S(t) \equiv \mathcal{H}_S^0(t) + \langle \mathcal{V}(t) \rangle_B \tag{31}$$

$$\mathcal{V}(t) \equiv \mathcal{V}^0(t) - \langle \mathcal{V}(t) \rangle_B \tag{32}$$

with the goal of solving the time-dependent Schrödinger equation

$$i\hbar \frac{\partial |\Psi(t)\rangle}{\partial t} = [\mathcal{H}_S(t) + \mathcal{H}_B(t) + \mathcal{V}(t)]|\Psi(t)\rangle = [\mathcal{H}_0(t) + \mathcal{V}(t)]|\Psi(t)\rangle \tag{33}$$

By introducing a unitary operator $U_0(t) = U_S(t)U_B(t)$

$$i\hbar \frac{d}{dt} U_0(t) = \mathcal{H}_0(t) U_0(t) \tag{34}$$

$$i\hbar \frac{d}{dt} U_S(t) = \mathcal{H}_S(t) U_S(t) \tag{35}$$

$$i\hbar \frac{d}{dt} U_B(t) = \mathcal{H}_B(t) U_B(t) \tag{36}$$

we can derive an "interaction picture" von Neumann equation

$$i\hbar \frac{d}{dt} \tilde{\rho}(t) = [\tilde{\mathcal{V}}(t), \tilde{\rho}(t)] \tag{37}$$

where

$$\tilde{\mathcal{V}}(t) = U_0^\dagger(t)\mathcal{V}(t)U_0(t) \tag{38}$$

$$\tilde{\rho}(t) = U_0^\dagger(t)\rho(t)U_0(t) \tag{39}$$

We assume the simple form of a harmonic system and bath, but allow fluctuations in the system and bath modes modeled by time-dependent frequencies

$$\mathcal{H}_S(t) = \hbar\omega_S(t)(a_S^\dagger a_S + 1/2) \tag{40}$$

$$\mathcal{H}_B(t) = \sum_\alpha \hbar\omega_\alpha(t)(a_\alpha^\dagger a_\alpha + 1/2) \tag{41}$$

The unitary operators generated by these Hamiltonians are

$$U_S(t) = e^{-i\int_0^t d\tau\omega_S(\tau)(a_S^\dagger a_S+1/2)} \tag{42}$$

$$U_B(t) = e^{-i\int_0^t d\tau\sum_\alpha \omega_\alpha(\tau)(a_\alpha^\dagger a_\alpha+1/2)} \tag{43}$$

and the time evolution of the annihilation operators is given by

$$U_S^\dagger(t)a_S U_S(t) = a_S e^{-i\int_0^t d\tau\omega_S(\tau)} \tag{44}$$

$$U_B^\dagger(t)a_\alpha U_B(t) = a_\alpha e^{-i\int_0^t d\tau\omega_\alpha(\tau)} \tag{45}$$

To simplify the evaluation of the force autocorrelation function, we assume that the temperature is low or the system mode frequency is high as a justification for the approximation. Substituting the above result into the force autocorrelation function calculated by the force operator, Eq. (22), we find

$$\langle\delta\mathcal{F}(t')\delta\mathcal{F}(t'')\rangle \simeq \frac{\hbar^2}{2}\sum_{\alpha,\beta}\frac{C_{S\alpha\beta}(t')C_{S\alpha\beta}(t'')}{\sqrt{\omega_\alpha(t')\omega_\beta(t')\omega_\alpha(t'')\omega_\beta(t'')}} \times e^{-i[\Theta_{\alpha\beta}(t')-\Theta_{\alpha\beta}(t'')]} \tag{46}$$

where

$$\Theta_S(t) = \int_0^t d\tau\omega_S(\tau) \tag{47}$$

$$\Theta_{\alpha\beta}(t) = \int_0^t d\tau[\omega_\alpha(\tau) + \omega_\beta(\tau)] \tag{48}$$

Substituting this approximation into the perturbation expansion Eqs. (15), (16), (17), we obtain our final result:

$$(\rho_S)_{00}(t) \simeq \frac{\hbar}{2}\sum_{\alpha,\beta}\int_0^t dt' \int_0^{t'} dt'' \frac{C_{S\alpha\beta}(t')C_{S\alpha\beta}(t'')}{\sqrt{\omega_S(t')\omega_\alpha(t')\omega_\beta(t')\omega_S(t'')\omega_\alpha(t'')\omega_\beta(t'')}} \times \cos\left\{\Theta_S(t') - \Theta_{\alpha\beta}(t') - \Theta_S(t'') + \Theta_{\alpha\beta}(t'')\right\} \tag{49}$$

which provides a dynamic correction to the previous formula [22]. The time-dependent parameters $\omega_S(t)$, $\omega_\alpha(t)$, and $C_{S\alpha\beta}(t)$ may be computed from a running trajectory using instantaneous normal mode analysis [36]. This result was first derived by Fujisaki and Stock [47], and applied to the VER dynamics of *N*-methylacetamide as described below. This correction eliminates the assumption that the bath frequencies are static on the VER timescale.

For the case of a static bath, the frequency and coupling parameters are time-independent and this formula reduces to the previous one-dimensional formula (when the off-resonant terms are neglected) [22]:

$$(\rho_S)_{00}(t) \simeq \frac{\hbar}{2\omega_S}\sum_{\alpha,\beta}\frac{C_{S\alpha\beta}^2}{\omega_\alpha\omega_\beta}\frac{1-\cos[(\omega_S-\omega_\alpha-\omega_\beta)t]}{(\omega_S-\omega_\alpha-\omega_\beta)^2} \tag{50}$$

Note that Bakker derived a similar fluctuating Landau–Teller formula in a different manner [51]. It was successfully applied to molecular systems by Sibert and coworkers [52]. However, the above formula differs from Bakker's as (a) we use the instantaneous normal mode analysis to parameterize our expression and (b) we do not take the Markov limit. Our formula can describe both the time course of the density matrix and the VER rate.

Another point is that we use the cumulant-type approximation to calculate the dynamics. When we calculate an excited state probability, we use

$$(\rho_S)_{11}(t) = 1 - (\rho_S)_{00}(t) \simeq \exp\{-(\rho_S)_{00}(t)\} \tag{51}$$

Of course, this is valid for the initial process ($(\rho_S)_{00}(t) \ll 1$), but, at longer timescales, we take $(\rho_S)_{11}(t) \simeq \exp\{-(\rho_S)_{00}(t)\}$ because the naive formula $(\rho_S)_{11}(t) = 1 - (\rho_S)_{00}(t)$ can be negative, which is unphysical [47].

C. Limitations of the VER Formulas and Comments

There are several limitations to the VER formulas derived above. The most obvious is that they are second-order perturbative formulas and rely on a short-time approximation. As far as we know, however, there exists no nonperturbative quantum mechanical treatment of VER applicable to *large* molecular systems. It is prohibitive to treat the full molecular dynamics quantum mechanically [53] for large molecules. Moreover, while there exist several mixed quantum classical methods [11]

that may be applied to the study of VER, there is no guarantee that such approximate methods work better than the perturbative treatment [54].

Another important limitation is the adaptation of a normal mode basis set, a natural choice for molecular vibrations. Because of the normal mode analysis, the computation can be burdensome. When we employ instantaneous normal mode analysis [36], there is a concern about the imaginary frequency modes. For the study of high-frequency modes, this may not be significant. However, for the study of low-frequency modes, the divergence of quantum (or classical) dynamics due to the presence of such imaginary frequency modes is a significant concern. For the study of low-frequency modes, it is more satisfactory to use other methods that do not rely on normal mode analysis such as semiclassical methods [55] or path integral methods [56].

We often use "empirical" force fields, with which quantum dynamics is calculated. However, it is well known that the force fields underestimate anharmonicity of molecular vibrations [57]. It is often desirable to use *ab initio* potential energy surfaces. However, such a rigorous approach is much more demanding. Lower levels of theory can fail to match the accuracy of some empirical potentials. As a compromise, approximate potentials of intermediate accuracy, such as QM/MM potentials [58], may be appropriate. We discuss this issue further in Sections IV.A and IV.C.

IV. APPLICATIONS OF THE VER FORMULAS TO VIBRATIONAL MODES IN BIOMOLECULES

We report our quantum dynamics studies of high-frequency modes in biomolecular systems using a variety of VER formulas described in Section III. The application of a variety of theoretical approaches to VER processes will allow for a relative comparison of theories and the absolute assessment of theoretical predictions compared with experimental observations. In doing so, we address a number of fundamental questions. What are the limitations of the static bath approximation for fast VER in biomolecular systems? Can the relaxation dynamics of a relaxing amide I vibration in a protein be accurately modeled as a one-dimensional system mode coupled to a harmonic bath? Can the "fluctuating bath" model accurately capture the system dynamics when the static picture of normal modes is not "good" on the timescale of the VER process? In Sections IV.A and IV.B, our main focus is the VER of excited amide I modes in peptides or proteins. In Section IV.C, we study some vibrational modes in porphyrin ligated to imidazole, which is a mimic of a heme molecule in heme proteins including myoglobin and hemoglobin.

A. *N*-Methylacetamide (NMA)

NMA is a well-studied small molecule (CH_3–CO–NH–CH_3) that serves as a convenient model of a peptide bond structure (–CO–NH–) in theory and experiment.

As in other amino acids, there is an amide I mode, localized on the CO bond stretch, which is a useful "reporter" of peptide structure and dynamics when probed by infrared spectroscopy. Many theoretical and experimental studies on amide I and other vibrational modes (amide II and amide III) have characterized how the mode frequencies depend on the local secondary structure of peptides or proteins [59, 60]. For the accurate description of frequencies and polarizability of these modes, see Refs. 15, 16 and 61–65. The main focus of these works is the frequency sensitivity of amide modes on the molecular configuration and environment. In this case, the amide mode frequencies are treated in a quantum mechanical way, but the configuration is treated classically. With a focus on interpreting mode frequency shifts due to configuration and environment, mode coupling between amide modes and other modes is often neglected. As we are mainly interested in VER or IVR dynamics of these modes, an accurate treatment of the mode coupling is essential.

Recent theoretical development of IVR dynamics in small molecules is summarized in Ref. 53. Leitner and Wolynes [7] utilized the concept of local random matrix to clarify the quantum aspects of such dynamics. The usefulness and applications of their approach are summarized both in Ref. 12 and in this volume [13]. However, these studies are focused on isolated molecules, whereas our main interest is in exploring quantum dynamics in a condensed phase. We take a step-by-step hierarchical approach. Starting from the isolated NMA molecule, we add several water molecules to form NMA–water clusters, and finally treat the condensed phase NMA–water system (see Fig. 3). With increasing complexity of our model, the accuracy of our theory, including the quality of the potential energy surface, and the accuracy of the quantum dynamics must diminish. As such, the principal focus of our account is a careful examination and validation of our procedures through comparison with accurate methods or experiments.

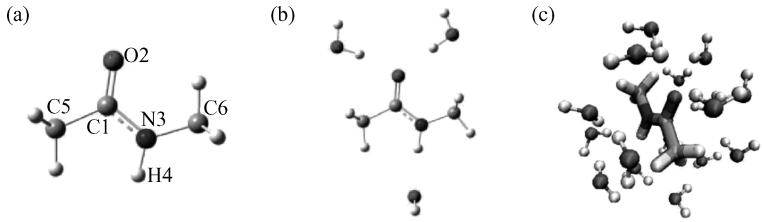

Figure 3. Representation of three models employed for the study of VER dynamics in *N*-methylacetamide. (**a**) NMA, (**b**) NMA with three solvating water, and (**c**) NMA with first solvation shell derived from simulations in bulk water. ((**a** and **b**) Reproduced with permission from Ref. 72. Copyright 2009 by the American Chemical Society. (**c**) Reproduced with permission from Ref. 47. Copyright 2009 by the American Institute of Physics.)

1. N-Methylacetamide in Vacuum

In our studies of isolated NMA [66, 67], we have employed both accurate potential energy surface and accurate quantum dynamics methods to explore the timescale and mechanism of VER. From the anharmonic frequency calculations and comparison to experiment [68], we concluded that B3LYP/6-31G(d) is a method of choice for computation of the electronic ground state potential surface, considering both accuracy and feasibility. For other treatments at differing levels of theory of quantum chemical calculation on NMA, see Refs. 57, 69, 70. After the construction of an accurate potential surface, there are several tractable approaches for treating the quantum dynamics for this system. The most accurate is the vibrational configuration interaction (VCI) method based on vibrational self-consistent field (VSCF) basis sets (see Refs. 48, 49, 66, 67 for details). We employed the Sindo code developed by Yagi [50]. The numerical results for the VCI calculation are shown in Fig. 4 and compared with the prediction based on the perturbative formula [Eq. (50)] and classical calculations as done in Ref. 42. Both approximate methods seem to work well, but there are caveats. The perturbative formula works only at short timescales. There is ambiguity for the classical simulation regarding how the zero point energy correction should be included (see Stock's papers [71]). The main results for a singly deuterated NMA (NMA-d_1) are (1) the relaxation time appears to be subpicoseconds, (2) as NMA is a small molecule, there is a recurrent phenomenon, (3) the dominant relaxation pathway involves three bath

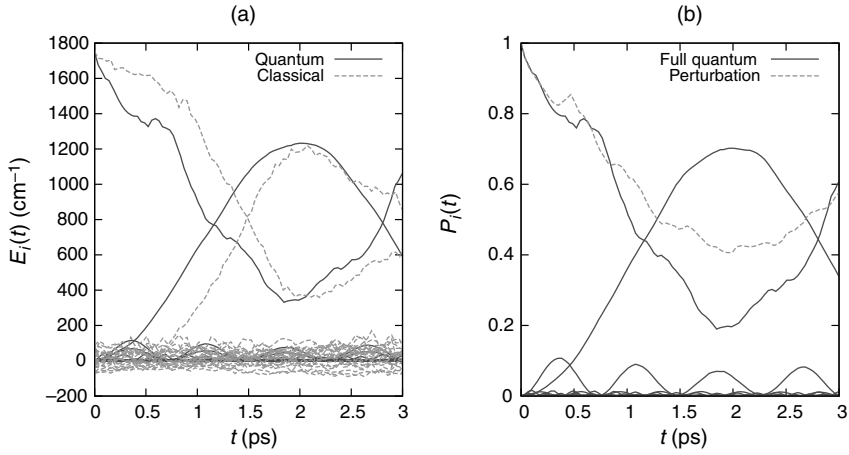

Figure 4. (**a**) Time evolution of the energy content of the initially excited amide I mode as well as all the remaining modes of *N*-methylacetamide. Quantum (solid lines) and classical (broken lines) calculations obtained at the DFT/B3LYP level of theory are compared. (**b**) Comparison of the VCI calculation (solid lines) with the result of the perturbative calculation (broken lines) for the reduced density matrix. (Reproduced with permission from Ref. 67. Copyright 2009 by Wiley–Interscience.)

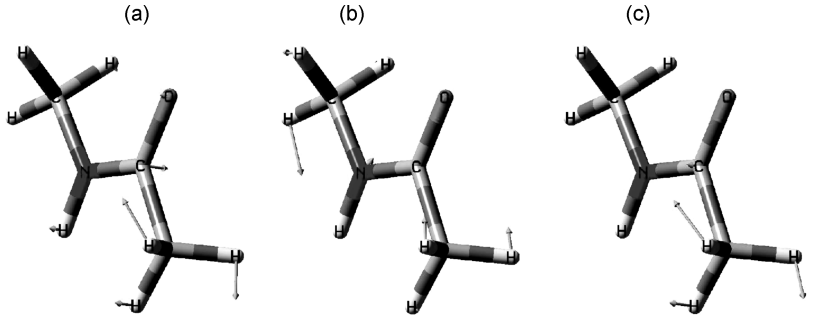

Figure 5. The dominant bath vibrational modes coupled to the amide I mode calculated on the B3LYP/6-31G(d) potential energy surface. (Reproduced with permission from Ref. 66. Copyright 2009 by Elsevier.)

modes as shown in Fig. 5, and (4) the dominant pathways can be identified and characterized by the following Fermi resonance parameter [66, 67]:

$$\eta \equiv \left| \frac{\langle i|\Delta V|f\rangle}{\Delta E} \right| \propto \left| \frac{C_{Skl}}{\hbar(\omega_S - \omega_k - \omega_l)} \right| \sqrt{\frac{\hbar}{2\omega_S}} \sqrt{\frac{\hbar}{2\omega_k}} \sqrt{\frac{\hbar}{2\omega_l}} \tag{52}$$

where $\langle i|\Delta V|f\rangle$ is the matrix element for the anharmonic coupling interaction and $\Delta E = \hbar(\omega_S - \omega_k - \omega_l)$ is the resonance condition (frequency matching) for the system and two bath modes. Both the resonant condition (ΔE) and anharmonic coupling elements (C_{Skl}) play a role, but we found that the former affects the result more significantly. This indicates that, for the description of VER phenomena in molecules, accurate calculation of the harmonic frequencies is more important than the accurate calculation of anharmonic coupling elements. This observation is the basis for the development and application of the multiresolution methods for anharmonic frequency calculations [45, 73].

2. *N-Methylacetamide/Water Cluster*

We next examine a somewhat larger system, NMA in a water cluster [72], an interesting and important model system for exploring the response of amide vibrational modes to "solvation" [62]. The system size allows for an *ab initio* quantum mechanical treatment of the potential surface at a higher level of theory, B3LYP/aug-cc-pvdz, relative to the commonly employed B3LYP/6-31G(d). The enhancement in the level of theory significantly improves the quality of the NMA–water interaction, specifically the structure and energetics of hydrogen bonding. Since there are at most three hydrogen bonding sites in NMA, it is natural to configure three water molecules around NMA as a minimal model of "full solvation."

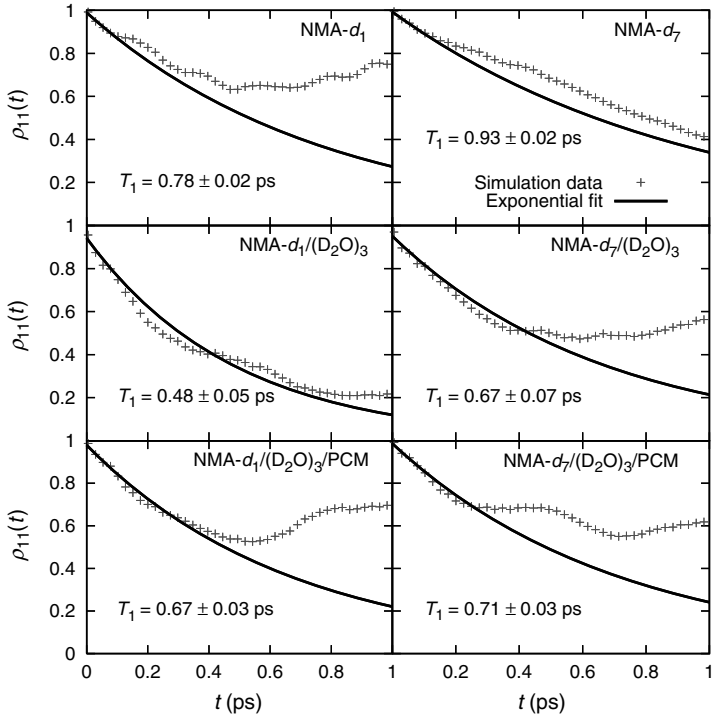

Figure 6. Time evolution of the density matrix for the amide I mode in the NMA–water cluster system after $v = 1$ excitation. The derived vibrational energy relaxation time constants T_1 are also provided. (Reproduced with permission from Ref. 72. Copyright 2009 by the American Chemical Society.)

See Fig. 3(b). NMA–water hydrogen bonding causes the frequency of the amide I mode to redshift. As a result, the anharmonic coupling between the relaxing mode and the other bath modes will change relative to the case of the isolated NMA. Nevertheless, we observe that the VER timescale remains subpicosecond as is the case for isolated NMA (Fig. 6). Though there are intermolecular (NMA–water) contributions to VER, they do not significantly alter the VER timescale. Another important finding is that the energy pathway from the amide I to amide II mode is "open" for the NMA–water cluster system. This result is in agreement with experimental results by Tokmakoff and coworkers [74] and recent theoretical investigation [16]. Comparison between singly (NMA-d_1) and fully (NMA-d_7) deuterated cases shows that the VER timescale becomes somewhat longer for the case of NMA-d_7 (Fig. 6). We also discuss this phenomenon below in the context of the NMA/solvent water system.

3. *N-Methylacetamide in Water Solvent*

Finally, we consider the condensed phase system of NMA in bulk water [22, 47, 58]. We attempt to include the full dynamic effect of the system by generating many configurations from molecular dynamics simulations and using them to ensemble average the results. Note that in the previous examples of isolated NMA and NMA/water clusters, only one configuration at a local minimum of the potential surface was used. On the other hand, the potential energy function used is not so accurate as in the previous examples as it is not feasible to include many water molecules at a high level of theory. We have used the CHARMM force field to calculate the potential energy and to carry out molecular dynamics simulations.

All simulations were performed using the CHARMM simulation program package [24] and the CHARMM22 all-atom force field [75] was employed to model the solute NMA-d_1 and the TIP3P water model [76] with doubled hydrogen masses to model the solvent D_2O. We also performed simulations for fully deuterated NMA-d_7. The peptide was placed in a periodic cubic box of $(25.5\ \text{Å})^3$ containing 551 D_2O molecules. All bonds containing hydrogens were constrained using the SHAKE algorithm [77]. We used a 10 Å cutoff with a switching function for the nonbonded interaction calculations. After a standard equilibration protocol, we ran a 100 ps NVT trajectory at 300 K, from which 100 statistically independent configurations were collected.

We first employed the simplest VER formula [Eqs.(50) and (51)] [22] as shown in Fig. 7. We truncated the system including only NMA and several water molecules around NMA with a cutoff distance, taken to be 10 Å. For reasons of computational

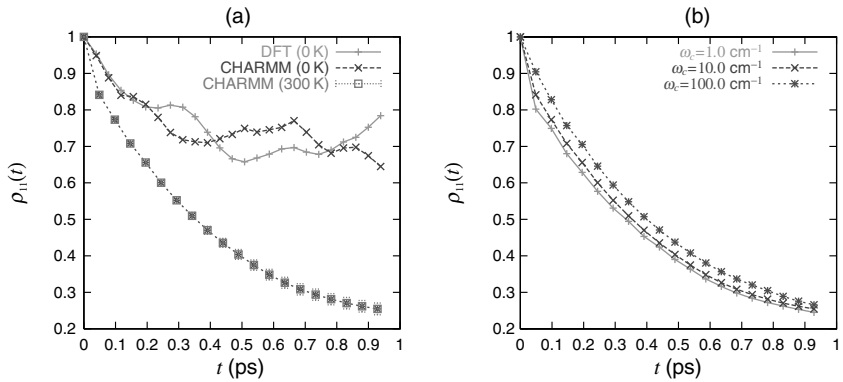

Figure 7. (**a**) Comparison of the calculation of the ρ_{11} element of the reduced density matrix at different levels of theory. (**b**) Calculation of the density matrix with different cutoff frequencies. (Reproduced with permission from Ref. 22. Copyright 2009 by the American Institute of Physics.)

feasibility, we only calculated the normal modes and anharmonic coupling elements within this subsystem.

A number of important conclusions were drawn from these calculations.

1. The inclusion of "many" solvating water molecules induces the irreversible decay of the excess energy as well as the density matrix elements (population). The important observation is that the VER behavior does not severely depend on the cutoff distance (if it is large enough) and the cutoff frequency. The implication is that if we are interested in a localized mode such as the amide I mode in NMA, it is enough to use an NMA/water cluster system to totally describe the initial process of VER. In a subsequent study, Fujisaki and Stock used only 16 water molecules surrounding NMA (hydrated water) and found reasonable results [47].
2. Comparison of the two isolated NMA calculations suggests that the CHARMM force field works well compared to results based on DFT calculations. This suggests that the use of the empirical force field in exploring VER of the amide I mode may be justified.
3. There is a classical limit of this calculation [22], which predicts a slower VER rate close to Nguyen–Stock's quasiclassical calculation [42]. This finding was explored further by Stock [78], who derived a novel quantum correction factor based on the reduced model, Eq. (2).

In these calculations, many solvating water configurations were generated using MD simulations. As such, information characterizing dynamic fluctuation in the environment is ignored. Fujisaki and Stock further improved the methodology to calculate VER [47] by taking into account the dynamic effects of the environment through the incorporation of time-dependent parameters, such as the normal mode frequencies and anharmonic coupling, derived from the MD simulations as shown in Fig. 8. Their method is described in Section III.B, and was applied to the same NMA/solvent water system. As we are principally concerned with high-frequency modes, and the instantaneous normal mode frequencies can become unphysical, we adopted a partial optimization strategy. We optimized the NMA under the influence of the solvent water at a *fixed* position. (For a different strategy, see Ref. 79.) The right panels of Fig. 8 show the numerical result of the optimization procedure. Through partial optimization, the fluctuations of the parameters become milder than the previous calculations that employed instantaneous normal modes.

The population dynamics calculated by the extended VER formula Eq. (49) are shown in Fig. 9. We see that both partial optimization and dynamical averaging affect the result. The "dynamic" formula, Eq. (49), leads to smaller fluctuations in the results for the density matrix. Apparently, dynamic averaging smoothens the resonant effect, stemming from the frequency difference in the denominator of Eq. (50). For the NMA/solvent water system, the time-averaged value of the

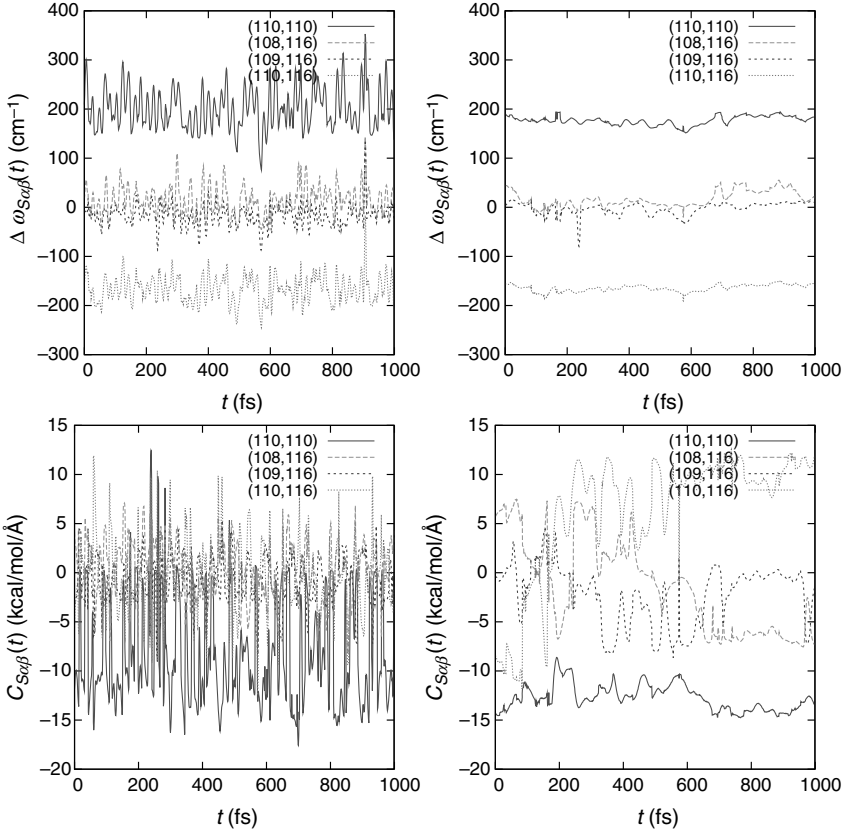

Figure 8. Time evolution of the vibrational dynamics of NMA in D_2O obtained from instantaneous normal mode analysis with (**right**) and without (**left**) partial energy minimization. Shown are (**upper panels**) the frequency mismatch $\Delta\omega_{S\alpha\beta}(t) = \omega_S(t) - \omega_\alpha(t) - \omega_\beta(t)$, for several resonant bath mode combinations, and (**lower panels**) the corresponding third-order anharmonic couplings, $C_{S\alpha\beta}(t)$. (Reproduced with permission from Ref. 47. Copyright 2009 by the American Institute of Physics.)

Fermi resonance parameter, Eq. (52), can be utilized to clarify the VER pathways as in the case of isolated NMA [47]. It was shown that the hydrating water (the number of waters is 16) is enough to fully describe the VER process at the initial stage ($\simeq$0.5 ps). The predictions of the VER rates for the two deuterated cases, NMA-d_1 and NMA-d_7, are in good agreement with experiment and also with the NMA/water cluster calculations [72]. Though the dynamic effect is modest in the case of the NMA/solvent water system, the dynamic formula is recommended when variations in the system parameters due to the fluctuating environment must be taken into account.

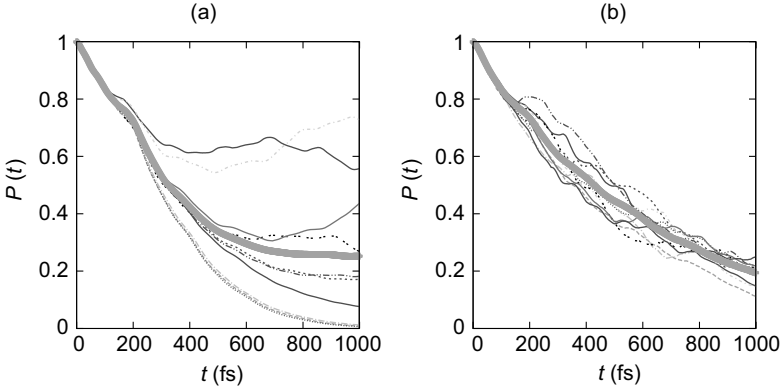

Figure 9. VER calculations of amide I mode population $P(t)$ of NMA with use of instantaneous normal mode analysis and partial energy minimization. Shown are results from (**a**) the inhomogeneous averaging approximation and (**b**) dynamical averaging. Thick lines represent the ensemble averaged population dynamics, whereas solid lines represent each contribution from a single trajectory. (Reproduced with permission from Ref. 47. Copyright 2009 by the American Institute of Physics.)

B. Cytochrome *c* in Water

Cytochrome c, one of heme proteins, has been used in experimental and theoretical studies of VER [21, 80–85]. Importantly, spectroscopy and simulation have been used to explore the timescales and mechanism of VER of CH stretching modes [21, 85]. Here we examine VER of amide I modes in cytochrome *c* [23]. Distinct from previous studies [21] that employed a static local minimum of the system, we use the dynamical trajectory; in the previous study, the water degrees of freedom were excluded, whereas in this study some hydrating water has been taken into account.

We used the trajectory of cytochrome *c* in water generated by Bu and Straub [85]. To study the local nature of the amide I modes and the correspondence with experiment, we isotopically labeled four specific CO bonds, typically $C^{12}O^{16}$ as $C^{14}O^{18}$. In evaluating the potential energy in our instantaneous normal mode analysis, we truncated the system with an amide I mode at the center using a cutoff ($\simeq$10 Å), including both protein and water. Following INM analysis, we used Eq. (50) to calculate the time course of the density matrix. The predicted VER is single exponential in character with timescales that are subpicosecond with relatively small variations induced by the different environments of the amide I modes (see Fig. 10 and Table I in Ref. 23 for numerical values of the VER timescales). To identify the principal contributions to the dependence on the environment, we examined the VER pathways and the roles played by protein and water degrees of freedom in VER. Our first conclusion is that, for the amide I modes buried in the protein (α-helical regions), the water contribution is less than that for the amide I modes exposed to water (loop regions). This finding is important because only

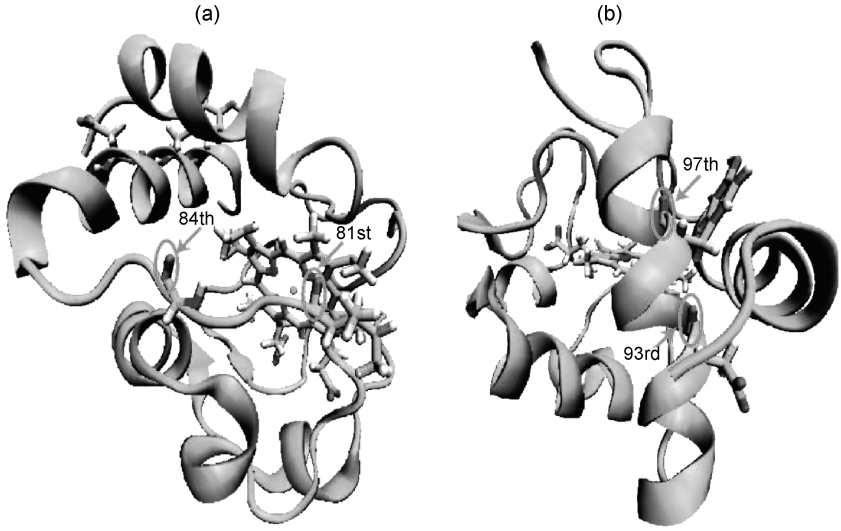

Figure 10. (**a**) 81st and 84th residues of cytochrome *c* in a loop region. (**b**) 93rd and 97th residues of cytochrome *c* in an α-helical region. The cartoon represents the protein using a licorice model to identify the four residues. (The water molecules are excluded for simplicity.) (Reproduced with permission from Ref. 23. Copyright 2009 by the American Chemical Society.)

a total VER timescale is accessible in experiment. With our method, the energy flow pathways into protein or water can be clarified.

Focusing on the resonant bath modes, we analyzed the anisotropy of the energy flow, as shown in Fig. 11, where the relative positions of bath modes participating in VER are projected on the spherical polar coordinates (θ, ϕ) centered on the CO bond involved in the amide I mode, which represents the principal z-axis (see Fig. 1 in Ref. 23). The angle dependence of the energy flow from the amide I mode to water is calculated from the normal mode amplitude average, and not directly related to experimental observables. As expected, energy flow is observed in the direction of solvating water. However, that distribution is not spatially isotropic and indicates preferential directed energy flow. These calculations demonstrate the power of our theoretical analysis in elucidating pathways for spatially directed energy flow of fundamental importance to studies of energy flow and signaling in biomolecules and the optimal design of nanodevices (see summary and discussion for more detail).

C. Porphyrin

Our last example is a modified porphyrin [86]. We have carried out systematic studies of VER in the porphyrin–imidazole complex, a system that mimics the active site of the heme protein, myoglobin. The structure of myoglobin was first

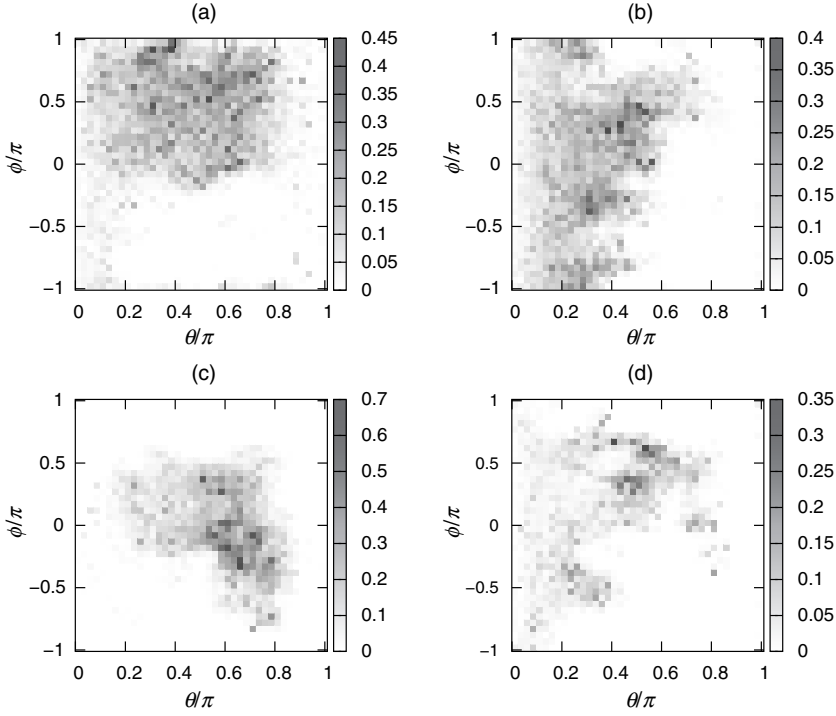

Figure 11. Angular excitation functions for the resonant normal modes of water for the (**a**) 81st, (**b**) 84th, (**c**) 93rd, and (**d**) 97th residues, represented in arbitrary units. (Reproduced with permission from Ref. 23. Copyright 2009 by the American Chemical Society.)

determined in 1958 [87]. Experimental and computational studies exploring the dynamics of myoglobin led to the first detailed picture of how fluctuations in a protein structure among a multitude of "conformational substate" support protein function [88]. Time-resolved spectroscopic studies [17] coupled with computational studies have provided a detailed picture of timescale and mechanism for energy flow in myoglobin and its relation to function. Karplus and coworkers developed the CHARMM force field [24] for heme and for amino acids for the study of myoglobin, and a particular focus on the dissociation and rebinding of ligands such as CO, NO, and O_2 [90]. The empirical force field appears to provide an accurate model of heme structure and fluctuations, however, we have less confidence in the accuracy of anharmonicity and mode coupling on the force field. Furthermore, the dependence on spin state is important to the proper identification of the electronic ground-state potential energy surface.

We carried out *ab initio* calculations for a heme-mimicking molecule, iron–porphin ligated to imidazole, abbreviated as FeP-Im. See Fig. 12 for the optimized

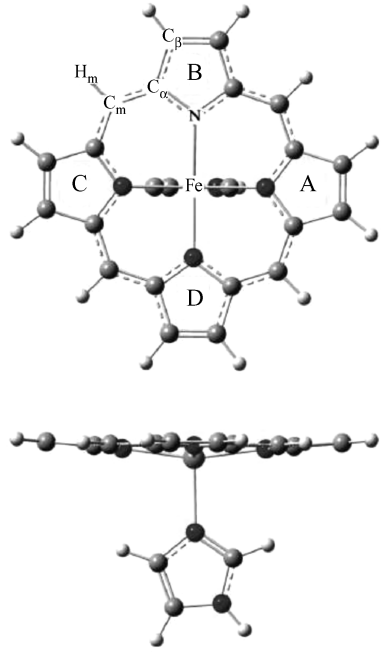

Figure 12. Optimized structure of FeP-Im (quintuplet $S = 2$ spin configuration) at the UB3LYP/6-31G(d) level of theory. (Reproduced with permission from Ref. 86. Copyright 2009 by the American Institute of Physics.)

structure. We employed the UB3LYP/6-31G(d) level of theory as in the case of the isolated NMA [66, 67], but carefully investigated the spin configurations. We identified the quintuplet ($S = 2$) as the electronic ground state, in accord with experiment. Our study of VER dynamics on this quintuplet ground-state potential energy surface is summarized here. Additional investigations of the VER dynamics on the PES corresponding to other spin configurations as well as different heme models are described elsewhere [86].

A series of elegant pioneering experimental studies have provided a detailed picture of the dynamics of the ν_4 and ν_7 modes, in-plane modes of the heme (see Fig. 13), following ligand photodissociation in myoglobin. Using time-resolved resonance Raman spectroscopy, Mizutani and Kitagawa observed mode-specific excitation and relaxation [18, 89]. Interestingly, these modes decay on different timescales. The VER timescales are $\sim$1.0 ps for the ν_4 mode and $\sim$2.0 ps for the ν_7 mode. Using a sub-10 fs pulse, Miller and coworkers extended the range of the coherence spectroscopy up to 3000 cm^{-1} [91]. The heme ν_7 mode was found to be most strongly excited following Q band excitation. By comparing to the deoxy-Mb spectrum, they demonstrated that the signal was derived from

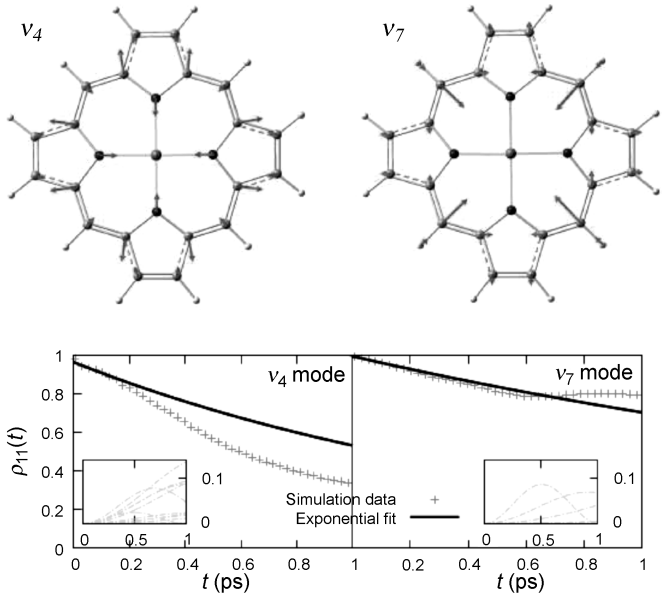

Figure 13. Time course of the ρ_{11} element of the reduced density matrix for ν_4 and ν_7 excitations of $v = 1$. For the explanation of the insets, refer to Ref. 89. (Reproduced with permission from Ref. 86. Copyright 2009 by the American Institute of Physics.)

the structural transition from the six-coordinate to the five-coordinate heme. Less prominent excitation of the ν_4 mode was also observed. The selective excitation of the ν_7 mode, following excitation of out-of-place heme doming, led to the intriguing conjecture that there may be directed energy transfer of the heme excitation to low-frequency motions connected to backbone displacement and to protein function. The low-frequency heme modes ($<$400 cm^{-1}) have been studied using femtosecond coherence spectroscopy with a 50 fs pulse [92]. A series of modes at $\sim$40, $\sim$80, $\sim$130, and $\sim$170 cm^{-1} were observed for several myoglobin derivatives. The couplings between these modes were suggested. It is a long-term goal of our studies to understand, at the mode-specific level, how the excess energy flow due to ligand dissociation leads to the selective excitation of ν_4 and ν_7 modes.

In our study, we ignore the transition in spin state that occurs upon ligand photodissociation and the associated electron–nuclear coupling that will no doubt be essential to an understanding of the "initial state" of the ν_4 and ν_7 vibrations following ligand photodissociation. Our focus was on the less ambitious but important question of vibrational energy flow on the ground-state ($S = 2$) surface following excitation resulting from photodissociation. We employed time-dependent perturbation theory, Eq. (50), to model the mode-specific relaxation dynamics. The initial

decay process of each system mode was fitted by a single-exponential function. The time constant of $\simeq$1.7 ps was derived for the ν_4 mode and $\simeq$2.9 ps for the ν_7 mode. These theoretical predictions, which make no assumptions regarding the VER mechanism, agree well with previous experimental results of Mizutani and Kitagawa for MbCO [18].

Vibrational energy transfer pathways were identified by calculating the third-order Fermi resonance parameters, Eq. (52). For the excited ν_4 and ν_7 modes, the dominant VER pathways involve porphin out-of-plane motions as energy accepting doorway modes. Importantly, no direct energy transfer between the ν_4 and ν_7 modes was observed. Cooling of the five Fe-oop (Fe-out-of-plane) modes, including the functionally important heme doming motion and Fe-Im stretching motion, takes place on the picosecond timescale. All modes dissipate vibrational energy through couplings, weaker or stronger, with low-frequency out-of-plane modes involving significant imidazole ligand motion. It has been suggested that these couplings trigger the delocalized protein backbone motion, important for protein function, which follows ligand dissociation in Mb.

The γ_7 mode, a porphin methine wagging motion associated with Fe-oop motion, is believed to be directly excited following ligand photodissociation in MbCO. The coupling of this mode to lower frequency bath modes is predicted to be very weak. However, its overtone is strongly coupled to the ν_7 mode, forming an effective energy transfer pathway for relaxation on the electronic ground-state and excited-state surfaces. This strong coupling suggests a possible mechanism of excitation of the ν_7 mode through energy transfer from the γ_7 mode. That mechanism is distinctly different from direct excitation together with Fe-oop motion of the ν_4 mode and supports earlier conjectures of mode-specific energy transfer following ligand dissociation in myoglobin [18, 91].

V. SUMMARY AND DISCUSSION

This chapter provides an overview of our recent work on the application of the non-Markovian theory of vibrational energy relaxation to a variety of systems of biomolecular interest, including protein backbone mimicking amide I modes in *N*-methylacetamide (in vacuum, in water cluster, and in solvent water), amide I modes in solvated cytochrome *c*, and vibrational modes in a heme-mimicking porphyrin ligated to imidazole. We calculated the VER timescales and mechanisms using Eq. (49), incorporating a fluctuating bath, and Eq. (50), using a static bath approximation, and compared them with experiment when available. The theory is based on the reduced model using normal mode concepts with third- and fourth-order anharmonicity, Eq. (2). Applying the simple time-dependent perturbation theory, and ensemble averaging the resulting density matrix, a non-Markovian theory of VER was obtained. We extended the previous theory due to Fujisaki et al. [22] to

more general situations (1) where the relaxing "system" has a multimode character and (2) when the system parameters depend on time [47]. We also discussed the limitations of our VER formulas related to the assumptions upon which the earlier theories are based.

We are now in a position to discuss the future aspects of our work, and the connection to other biomolecular systems or nanotechnological devices.

- *Relation to Enzymatic Reaction*. The role of vibrational motions in the mechanism of enzymatic reactions remains controversial [93]. In enzymology, the characterization of the enzymatic reaction rate is essential. Kinetic information is typically derived from substrate–enzyme kinetics experiments. In numerical simulations, the free energy calculation combined with transition state theory is the most powerful and practical way to compute reaction rates. As enzymatically catalyzed reactions typically involve chemical bond breaking and formation, QM/MM-type methods should be employed. Warshel and Parson have examined this issue for several decades and concluded that characterizing the free energy barrier is the most important consideration, noting that the electrostatic influence from the protein (enzyme) plays a key role [94]. However, Hammes-Schiffer and coworkers have identified important situations in which VER might play a role in controlling the rate of enzymatic reactions [93]. Furthermore, Hynes and coworkers applied the Grote–Hynes theory to the enzymatic reactions and investigated the dynamic role of the environment [6]. These recent studies indicate the importance of incorporating vibrational energy flow and dynamics as part of a complete understanding of enzyme kinetics.
- *Relation to Conformational Change*. The relation between vibrational excitation/relaxation and conformational change of molecules is intriguing in part because of the possible relation to the optimal control of molecular conformational change using tailored laser pulses. It is well known that there are dynamic corrections to the RRKM reaction rate, the simplest being

$$k(E)/k_{\mathrm{RRKM}}(E) = (1 + \nu_R/k_{\mathrm{IVR}}(E))^{-1} \tag{53}$$

  where ν_R is the intrinsic frequency of a reaction coordinate, $k_{\mathrm{IVR}}(E)$ is a microcanonical IVR rate, and $k_{\mathrm{IVR}}(E)$ is the RRKM reaction rate [3–5]. Several modifications to this formula are summarized in Ref. 12. It is obvious that VER affects how a molecule changes its shape. However, this is a "passive" role of VER. Combining RRKM theory and the local random matrix theory [7], Leitner and coworkers theoretically studied the active role of vibrational excitations on conformational change of a peptide-like molecule (called NATMA) [95]. There are two particular modes (NH stretching) in NATMA, and they found that the final product depends on which vibrational

mode is excited [96]. For the same system, Teramoto and Komatsuzaki further refined the calculation by employing *ab initio* potential energy surface [97]. A possibility to control molecular configurations of peptides or proteins using laser pulses should be pursued and some experimental attempts have already begun [20, 98, 99].

Another interesting attempt should be to address mode-specific energy flow associated with structural change. Recently, Ikeguchi et al. [100] developed a linear response theory for conformational changes of biomolecules, which is summarized in another chapter of this volume [37]. Though the original formulation is based on a static picture of the linear response theory (susceptibility), its nonequilibrium extension may be used to explore the relation between energy flow and conformational change in proteins. In addition, Koyama et al. [101] devised a method based on principal component analysis for individual interaction energies of a peptide (and water) and found an interesting correlation between the principal modes and the direction of conformational change [101].

- *Relation to Signal Transduction in Proteins*. Though signal transduction in biology mainly denotes the information transfer processes carried out by a series of proteins in a cell, it can be interesting and useful to study the information flow in a single protein, which should be related to vibrational dynamics. Straub and coworkers [41] studied such energy flow pathways in myoglobin and found particular pathways from heme to water, later confirmed experimentally by Kitagawa and coworkers [102] and Champion and coworkers [92]. Ota and Agard [103] devised a novel simulation protocol, *anisotropic thermal diffusion*, and found a particular energy flow pathway in the PDZ domain protein. Importantly, the pathway they identified is located near the conserved amino acid region in the protein family previously elucidated using information theoretic approach by Lockless and Ranganathan [104]. Sharp and Skinner [105] proposed an alternative method, *pump–probe MD*, and examined the same PDZ domain protein, identifying alternative energy flow pathways. Using linear response theory describing thermal diffusion, Ishikura and Yamato [106] discussed the energy flow pathways in photoactive yellow protein. This method was recently extended to the frequency domain by Leitner and applied to myoglobin dimer [107]. Though the energy flow mentioned above occurs quite rapidly ($\sim$ps), there are time-resolved spectroscopic methods to detect these pathways *in vitro* [20]. Comparison between theory and experiment will help clarify the biological role of such energy flow in biomolecular systems.
- *Exploring the Role of VER in Nanodevice Design*. Applications of the methods described in this chapter are not limited to biomolecular systems. As

mentioned in Section I, heat generation is always an issue in nanotechnology, and an understanding of VER in molecular devices can potentially play an important role in optimal device design. The estimation of thermal conductivity in such devices is a good starting point recently pursued by Leitner [12]. Nitzan and coworkers studied thermal conduction in a molecular wire using a simplified model [108]. It will be interesting to add more molecular detail to such model calculations. Electronic conduction has been one of the main topics in nanotechnology and mesoscopic physics [109], and heat generation during electronic current flow is an additional related area of importance.

- *VER in a Confined Environment*. We have found evidence for spatially anisotropic vibrational energy flow with specific pathways determined by resonance and coupling conditions. It was shown for amide I modes in cytochrome *c* that VER may depend on the position of the probing modes [23], making it useful for the study of inhomogeneity of the environment. For example, an experimental study of VER in a reverse micelle environment [110], fullerene, nanotube, membrane, or on atomic or molecular surfaces [111] may all be approached using methods described in this chapter.
- *Anharmonic Effects in Coarse-Grained Models of Proteins*. Recently Togashi and Mikhailov studied the conformational relaxation of elastic network models [112]. Though the model does not explicitly incorporate anharmonicity, small anharmonicity exists, resulting in interesting physical behavior relevant to biological function. Sanejouand and coworkers added explicit anharmonicity to the elastic network models and studied the energy storage [113] through the lens of "discrete breather" ideas from nonlinear science [114]. Surprisingly, they found that the energy storage may occur in the active sites of proteins. It remains to be seen whether their conjecture will hold for all-atom models of the same system.

Acknowledgments

The authors gratefully acknowledge fruitful and enjoyable collaborations with Prof. G. Stock, Prof. K. Hirao, and Dr. K. Yagi, the results of which form essential contributions to this chapter. We thank Prof. David M. Leitner, Prof. Akinori Kidera, Prof. Mikito Toda, Dr. Motoyuki Shiga, Dr. Sotaro Fuchigami, and Dr. Hiroshi Teramoto for useful discussions. The authors are grateful for the generous support of this research by the National Science Foundation (CHE-0316551 and CHE-0750309) and Boston University's Center for Computational Science. This research was supported by Research and Development of the Next-Generation Integrated Simulation of Living Matter, a part of the Development and Use of the Next-Generation Supercomputer Project of the Ministry of Education, Culture, Sports, Science and Technology (MEXT).

References

1. D. M. Leitner and J. E. Straub, eds., *Proteins: Energy, Heat and Signal Flow*, Taylor & Francis/CRC Press, London, 2009.

2. A. Nitzan, *Chemical Dynamics in Condensed Phase: Relaxation, Transfer, and Reactions in Condensed Molecular Systems*, Oxford University Press, Oxford, 2006.
3. J. I. Steinfeld, J. S. Francisco, and W. L. Hase, *Chemical Kinetics and Dynamics*, Prentice Hall, Inc., 1989.
4. G. D. Billing and K. V. Mikkelsen, *Introduction to Molecular Dynamics and Chemical Kinetics*, Wiley, 1996.
5. B. J. Berne, M. Borkovec, and J. E. Straub, *J. Phys. Chem.* **92**, 3711 (1988).
6. J. J. Ruiz-Pernia, I. Tunon, V. Moliner, J. T. Hynes, and M. Roca, *J. Am. Chem. Soc.* **130**, 7477 (2008).
7. D. M. Leitner and P. G. Wolynes, *Chem. Phys. Lett.* **280**, 411 (1997). S. Northrup and J. T. Hynes, *J. Chem. Phys.* **73**, 2700 (1980).
8. D. W. Oxtoby, *Adv. Chem. Phys.* **40**, 1 (1979); **47**, 487 (1981); *Annu. Rev. Phys. Chem.* **32**, 77 (1981). V. M. Kenkre, A. Tokmakoff, and M. D. Fayer, *J. Chem. Phys.* **101**, 10618 (1994).
9. R. Rey, K. B. Moller, and J. T. Hynes, *Chem. Rev.* **104**, 1915 (2004). K. B. Moller, R. Rey, and J. T. Hynes, *J. Phys. Chem. A* **108**, 1275 (2004).
10. C. P. Lawrence and J. L. Skinner, *J. Chem. Phys.* **117**, 5827 (2002); **117**, 8847 (2002); **118**, 264 (2003). A. Piryatinski, C. P. Lawrence, and J. L. Skinner, *J. Chem. Phys.* **118**, 9664 (2003); **118**, 9672 (2003). C. P. Lawrence and J. L. Skinner, *J. Chem. Phys.* **119**, 1623 (2003); **119**, 3840 (2003).
11. S. Okazaki, *Adv. Chem. Phys.* **118**, 191 (2001). M. Shiga and S. Okazaki, *J. Chem. Phys.* **109**, 3542 (1998); **111**, 5390 (1999). T. Mikami, M. Shiga, and S. Okazaki, *J. Chem. Phys.* **115**, 9797 (2001). T. Terashima, M. Shiga, and S. Okazaki, *J. Chem. Phys.* **114**, 5663 (2001). T. Mikami and S. Okazaki, *J. Chem. Phys.* **119**, 4790 (2003); **121**, 10052 (2004). M. Sato and S. Okazaki, *J. Chem. Phys.* **123**, 124508 (2005); **123**, 124509 (2005).
12. D. M. Leitner, *Adv. Chem. Phys.* **130B**, 205 (2005); *Phys. Rev. Lett.* **87**, 188102 (2001). X. Yu and D. M. Leitner, *J. Chem. Phys.* **119**, 12673 (2003); *J. Phys. Chem. B* **107**, 1689 (2003). D. M. Leitner, M. Havenith, and M. Gruebele, *Int. Rev. Phys. Chem.* **25**, 553 (2006). D. M. Leitner, *Annu. Rev. Phys. Chem.* **59**, 233 (2008).
13. D. M. Leitner, Y. Matsunaga, C. B. Li, T. Komatsuzaki, R. S. Berry, and M. Toda, *Adv. Chem. Phys.* **145**, 83–122 (2011).
14. V. Pouthier, *J. Chem. Phys.* **128**, 065101 (2008). V. Pouthier and Y. O. Tsybin, *J. Chem. Phys.* **129**, 095106 (2008). V. Pouthier, *Phys. Rev. E* **78**, 061909 (2008).
15. A. G. Dijkstra, T. la Cour Jansen, R. Bloem, and J. Knoester, *J. Chem. Phys.* **127**, 194505 (2007).
16. R. Bloem, A. G. Dijkstra, T. la Cour Jansen, and J. Knoester, *J. Chem. Phys.* **129** 055101 (2008).
17. P. Hamm, M. H. Lim, and R. M. Hochstrasser, *J. Phys. Chem. B* **102**, 6123 (1998). M. T. Zanni, M. C. Asplund, and R. M. Hochstrasser, *J. Chem. Phys.* **114**, 4579 (2001).
18. Y. Mizutani and T. Kitagawa, *Science* **278**, 443 (1997).
19. A. Pakoulev, Z. Wang, Y. Pang, and D. D. Dlott, *Chem. Phys. Lett.* **380**, 404 (2003). Y. Fang, S. Shigeto, N. H. Seong, and D. D. Dlott, *J. Phys. Chem. A* **113**, 75 (2009).
20. P. Hamm, J. Helbing, and J. Bredenbeck, *Annu. Rev. Phys. Chem.* **59**, 291 (2008).
21. H. Fujisaki, L. Bu, and J. E. Straub, *Adv. Chem. Phys.* **130B**, 179 (2005). H. Fujisaki and J. E. Straub, *Proc. Natl. Acad. Sci. USA* **102**, 6726 (2005). M. Cremeens, H. Fujisaki, Y. Zhang, J. Zimmermann, L. B. Sagle, S. Matsuda, P. E. Dawson, J. E. Straub, and F. E. Romesberg, *J. Am. Chem. Soc.* **128**, 6028 (2006).
22. H. Fujisaki, Y. Zhang, and J. E. Straub, *J. Chem. Phys.* **124**, 144910 (2006).
23. H. Fujisaki and J. E. Straub, *J. Phys. Chem. B* **111**, 12017 (2007).

24. B. R. Brooks, R. E. Bruccoleri, B. D. Olafson, D. J. States, S. Swaminathan, and M. Karplus, *J. Comput. Chem.* **4**, 187 (1983). A. D. MacKerell, Jr., B. Brooks, C. L. Brooks, III, L. Nilsson, B. Roux, Y. Won, and M. Karplus, in *The Encyclopedia of Computational Chemistry 1*. P. v.R. Schleyer, et al., eds., Wiley, Chichester, UK, 1998, pp. 271–277. B. R. Brooks, C. L. Brooks, III, A. D. Mackerell, Jr., L. Nilsson, R. J. Petrella, B. Roux, Y. Won, G. Archontis, C. Bartels, S. Boresch, A. Caflisch, L. Caves, Q. Cui, A. R. Dinner, M. Feig, S. Fischer, J. Gao, M. Hodoscek, W. Im, K. Kuczera, T. Lazaridis, J. Ma, V. Ovchinnikov, E. Paci, R. W. Pastor, C. B. Post, J. Z. Pu, M. Schaefer, B. Tidor, R. M. Venable, H. L. Woodcock, X. Wu, W. Yang, D. M. York, and M. Karplus, *J. Comput. Chem.* **30**, 1545 (2009).

25. M. J. Frisch, G. W. Trucks, H. B. Schlegel, G. E. Scuseria, M. A. Robb, J. R. Cheeseman, J. A. Montgomery, Jr., T. Vreven, K. N. Kudin, J. C. Burant, J. M. Millam, S. S. Iyengar, J. Tomasi, V. Barone, B. Mennucci, M. Cossi, G. Scalmani, N. Rega, G. A. Petersson, H. Nakatsuji, M. Hada, M. Ehara, K. Toyota, R. Fukuda, J. Hasegawa, M. Ishida, T. Nakajima, Y. Honda, O. Kitao, H. Nakai, M. Klene, X. Li, J. E. Knox, H. P. Hratchian, J. B. Cross, V. Bakken, C. Adamo, J. Jaramillo, R. Gomperts, R. E. Stratmann, O. Yazyev, A. J. Austin, R. Cammi, C. Pomelli, J. W. Ochterski, P. Y. Ayala, K. Morokuma, G. A. Voth, P. Salvador, J. J. Dannenberg, V. G. Zakrzewski, S. Dapprich, A. D. Daniels, M. C. Strain, O. Farkas, D. K. Malick, A. D. Rabuck, K. Raghavachari, J. B. Foresman, J. V. Ortiz, Q. Cui, A. G. Baboul, S. Clifford, J. Cioslowski, B. B. Stefanov, G. Liu, A. Liashenko, P. Piskorz, I. Komaromi, R. L. Martin, D. J. Fox, T. Keith, M. A. Al-Laham, C. Y. Peng, A. Nanayakkara, M. Challacombe, P. M. W. Gill, B. Johnson, W. Chen, M. W. Wong, C. Gonzalez, and J. A. Pople, Gaussian 03, Revision C.02, Gaussian, Inc., Wallingford, CT, 2004.

26. E. B. Wilson, Jr., J. C. Decius, and P. C. Cross, *Molecular Vibrations*, Dover, 1980.

27. Q. Cui and I. Bahar, eds., *Normal Mode Analysis: Theory and Applications to Biological and Chemical Systems*, Chapman & Hall/CRC Press, London, 2006.

28. N. Go, T. Noguchi, and T. Nishikawa, *Proc. Natl. Acad. Sci. USA* **80**, 3696 (1983). B. Brooks and M. Karplus, *Proc. Natl. Acad. Sci. USA* **80**, 6571 (1983).

29. D. van der Spoel, E. Lindahl, B. Hess, G. Groenhof, A. E. Mark and H. J. C. Berendsen, *J. Comput. Chem.* **26**, 1701 (2005).

30. D. A. Case, T. E. Cheatham, III, T. Darden, H. Gohlke, R. Luo, K. M. Merz, Jr., A. Onufriev, C. Simmerling, B. Wang, and R. Woods, *J. Comput. Chem.* **26**, 1668 (2005).

31. H. Wako, S. Endo, K. Nagayama, and N. Go, *Comput. Phys. Commun.* **91**, 233 (1995).

32. F. Tama, F.-X. Gadea, O. Marques, and Y.-H. Sanejouand, *Proteins* **41**, 1 (2000).

33. L. Mouawad and D. Perahia, *Biopolymers* **33**, 569 (1993).

34. M. M. Tirion, *Phys. Rev. Lett.* **77**, 1905 (1996).

35. T. Haliloglu, I. Bahar, and B. Erman, *Phys. Rev. Lett.* **79**, 3090 (1997).

36. M. Cho, G. R. Fleming, S. Saito, I. Ohmine, and R. M. Stratt, *J. Chem. Phys.* **100**, 6672 (1994). J. E. Straub and J.-K. Choi, *J. Phys. Chem.* **98**, 10978–10987 (1994). R. M. Stratt, *Acc. Chem. Res.* **28**, 201 (1995). T. Keyes, *J. Phys. Chem. A* **101**, 2921 (1997).

37. S. Fuchigami, H. Fujisaki, Y. Matsunaga, and A. Kidera, *Adv. Chem. Phys.* **145**, 35 (2011).

38. K. Moritsugu, O. Miyashita and A. Kidera, *Phys. Rev. Lett.* **85**, 3970 (2000); *J. Phys. Chem. B* **107**, 3309 (2003).

39. M. Toda, R. Kubo, and N. Saito, *Statistical Physics I: Equilibrium Statistical Mechanics*, 2nd ed., Springer, 2004.

40. I. Okazaki, Y. Hara, and M. Nagaoka, *Chem. Phys. Lett.* **337**, 151 (2001). M. Takayanagi, H. Okumura, and M. Nagaoka, *J. Phys. Chem. B* **111**, 864 (2007).

41. D. E. Sagnella and J. E. Straub, *J. Phys. Chem. B* **105**, 7057 (2001). L. Bu and J. E. Straub, *J. Phys. Chem. B* **107**, 10634 (2003); **107**, 12339 (2003). Y. Zhang, H. Fujisaki, and J. E. Straub, *J. Phys. Chem. B* **111**, 3243 (2007). Y. Zhang and J. E. Straub, *J. Phys. Chem. B* **113**, 825 (2009).
42. P. H. Nguyen and G. Stock, *J. Chem. Phys.* **119**, 11350 (2003). P. H. Nguyen and G. Stock, *Chem. Phys.* **323**, 36 (2006). P. H. Nguyen, R. D. Gorbunov, and G. Stock, *Biophys. J.* **91**, 1224 (2006). E. Backus, P. H. Nguyen, V. Botan, R. Pfister, A. Moretto, M. Crisma, C. Toniolo, O. Zerbe, G. Stock, and P. Hamm, *J. Phys. Chem. B* **112**, 15487 (2008). P. H. Nguyen, P. Derreumaux, and G. Stock, *J. Phys. Chem. B* **113**, 9340–9347 (2009).
43. X. Yu and D. M. Leitner, *J. Chem. Phys.* **119**, 12673 (2003). D. A. Lidar, D. Thirumalai, R. Elber, and R. B. Gerber, *Phys. Rev. E* **59**, 2231 (1999).
44. A. Roitberg, R. B. Gerber, R. Elber, and M. A. Ratner, *Science* **268**, 1319 (1995).
45. K. Yagi, S. Hirata, and K. Hirao, *Theor. Chem. Acc.* **118**, 681 (2007); *Phys. Chem. Chem. Phys.* **10**, 1781–1788 (2008).
46. K. Yagi, H. Karasawa, S. Hirata, and K. Hirao, *ChemPhysChem* **10**, 1442–1444 (2009).
47. H. Fujisaki and G. Stock, *J. Chem. Phys.* **129**, 134110 (2008).
48. S. Carter, S. J. Culik, and J. M. Bowman, *J. Chem. Phys.* **107**, 10458 (1997); S. Carter and J. M. Bowman, *J. Chem. Phys.* **108**, 4397 (1998).
49. S. Carter, J. M. Bowman, and N. C. Handy, *Theor. Chem. Acc.* **100**, 191 (1998).
50. K. Yagi, SINDO Version 1.3, 2006.
51. H. J. Bakker, *J. Chem. Phys.* **121**, 10088 (2004).
52. E. L. Sibert and R. Rey, *J. Chem. Phys.* **116**, 237 (2002). T. S. Gulmen and E. L. Sibert, *J. Phys. Chem. A* **109**, 5777 (2005). S. G. Ramesh and E. L. Sibert, *J. Chem. Phys.* **125**, 244512 (2006); **125**, 244513 (2006).
53. M. Gruebele and P. G. Wolynes, *Acc. Chem. Res.* **37**, 261 (2004). M. Gruebele, *J. Phys. Condens. Matter* **16**, R1057 (2004).
54. J. S. Bader and B. J. Berne, *J. Chem. Phys.* **100**, 8359 (1994).
55. Q. Shi and E. Geva, *J. Chem. Phys.* **118**, 7562 (2003); *J. Phys. Chem. A* **107**, 9059 (2003); **107**, 9070 (2003). B. J. Ka, Q. Shi, and E. Geva, *J. Phys. Chem. A* **109**, 5527 (2005). B. J. Ka and E. Geva, *J. Phys. Chem. A* **110**, 13131 (2006). I. Navrotskaya and E. Geva, *J. Phys. Chem. A* **111**, 460 (2007); *J. Chem. Phys.* **127**, 054504 (2007).
56. B. J. Berne and D. Thirumalai, *Annu. Rev. Phys. Chem.* **37**, 401 (1986). G. Krilov, E. Sim, and B. J. Berne, *Chem. Phys.* **268**, 21 (2001).
57. S. K. Gregurick, G. M. Chaban, and R. B. Gerber, *J. Phys. Chem. A* **106**, 8696 (2002).
58. M. Shiga, M. Tachikawa, and H. Fujisaki, unpublished.
59. S. Krimm and J. Bandekar, *Adv. Prot. Chem.* **38**, 181 (1986). A. Barth and C. Zscherp, *Q. Rev. Biophys.* **35**, 369 (2002).
60. H. Torii and M. Tasumi, *J. Chem. Phys.* **96**, 3379 (1992).
61. H. Torii and M. Tasumi, *J. Raman Spectrosc.* **29**, 81 (1998). H. Torii, *J. Phys. Chem. B* **111**, 5434 (2007); **112**, 8737 (2008).
62. S. A. Corcelli, C. P. Lawrence, and J. L. Skinner, *J. Chem. Phys.* **120**, 8107 (2004). J. R. Schmidt, S. A. Corcelli, and J. L. Skinner, *J. Chem. Phys.* **121**, 8887 (2004). S. Li, J. R. Schmidt, S. A. Corcelli, C. P. Lawrence, and J. L. Skinner, *J. Chem. Phys.* **124**, 204110 (2006).
63. S. Ham, S. Hahn, C. Lee, and M. Cho, *J. Phys. Chem. B* **109**, 11789 (2005). M. Cho, *Chem. Rev.* **108**, 1331 (2008). Y. S. Kim and R. M. Hochstrasser, *J. Phys. Chem. B* **113**, 8231 (2009).

64. W. Zhuang, D. Abramavicius, T. Hayashi, and S. Mukamel, *J. Phys. Chem. B* **110**, 3362 (2003). T. Hayashi, T. l.C. Jansen, W. Zhuang, and S. Mukamel, *J. Phys. Chem. A* **64**, 109 (2005). T. Hayashi and S. Mukamel, *J. Phys. Chem. B* **111**, 11032 (2007); *J. Mol. Liq.* **141**, 149 (2008).
65. R. D. Gorbunov, P. H. Nguyen, M. Kobus, and G. Stock, *J. Chem. Phys.* **126**, 054509 (2007). R. D. Gorbunov and G. Stock, *Chem. Phys. Lett.* **437**, 272 (2007). M. Kobus, R. D. Gorbunov, P. H. Nguyen, and G. Stock, *Chem. Phys.* **347**, 208 (2008).
66. H. Fujisaki, K. Yagi, K. Hirao, and J. E. Straub, *Chem. Phys. Lett.* **443**, 6 (2007).
67. H. Fujisaki, K. Yagi, J. E. Straub, and G. Stock, *Int. J. Quantum Chem.* **109**, 2047 (2009).
68. S. Ataka, H. Takeuchi, and M. Tasumi, *J. Mol. Struct.* **113**, 147 (1984).
69. M. Bounouar and Ch. Scheurer, *Chem. Phys.* **323**, 87 (2006).
70. A. L. Kaledin and J. M. Bowman, *J. Phys. Chem. A* **111**, 5593 (2007).
71. G. Stock and U. Müller, *J. Chem. Phys.* **111**, 65 (1999). U. Müller and G. Stock, *J. Chem. Phys.* **111**, 77 (1999).
72. Y. Zhang, H. Fujisaki, and J. E. Straub, *J. Phys. Chem. A* **113**, 3051 (2009).
73. G. Rauhut, *J. Chem. Phys.* **121**, 9313 (2004).
74. L. P. DeFlores, Z. Ganim, S. F. Ackley, H. S. Chung, and A. Tokmakoff, *J. Phys. Chem. B* **110**, 18973 (2006).
75. A. D. MacKerell, Jr., D. Bashford, M. Bellott, R. L. Dunbrack, J. D. Evanseck, M. J. Field, S. Fischer, J. Gao, H. Guo, S. Ha, D. Joseph-McCarthy, L. Kuchnir, K. Kuczera, F. T.K. Lau, C. Mattos, S. Michnick, T. Ngo, D. T. Nguyen, B. Prodhom, W. E. Reiher, B. Roux, M. Schlenkrich, J. C. Smith, R. Stote, J. E. Straub, M. Watanabe, J. Wiorkiewicz-Kuczera, D. Yin, and M. Karplus, *J. Phys. Chem. B* **102**, 3586 (1998).
76. W. L. Jorgensen, J. Chandrasekhar, J. Madura, R. W. Impey, and M. L. Klein, *J. Chem. Phys.* **79**, 926 (1983).
77. J.-P. Ryckaert, G. Ciccotti, and H. J.C. Berendsen, *J. Comput. Phys.* **23**, 327 (1977).
78. G. Stock, *Phys. Rev. Lett.* **102**, 118301 (2009).
79. K. Yagi and D. Watanabe, *Int. J. Quantum Chem.* **109**, 2080 (2009).
80. L. Bu and J. E. Straub, *J. Phys. Chem. B* **107**, 12339 (2003).
81. Y. Zhang and J. E. Straub, *J. Phys. Chem. B* **113**, 825 (2009).
82. P. Li, J. T. Sage, and P. M. Champion, *J. Chem. Phys.* **97**, 3214 (1992).
83. W. Wang, X. Ye, A. A. Demidov, F. Rosca, T. Sjodin, W. Cao, M. Sheeran, and P. M. Champion, *J. Phys. Chem. B* **104**, 10789 (2000).
84. M. Negrerie, S. Cianetti, M. H. Vos, J. Martin, and S. G. Kruglik, *J. Phys. Chem. B* **110**, 12766 (2006).
85. L. Bu and J. E. Straub, *Biophys. J.* **85**, 1429 (2003).
86. Y. Zhang, H. Fujisaki, and J. E. Straub, *J. Chem. Phys.* **130**, 025102 (2009). Y. Zhang and J. E. Straub, *J. Chem. Phys.* **130**, 095102 (2009); **130**, 215101 (2009).
87. J. C. Kendrew, G. Bodo, H. M. Dintzis, R. G. Parrish, H. Wyckoff, and D. C. Phillips, *Nature* **181**, 662 (1958).
88. H. Frauenfelder, S. G. Sligar, and P. G. Wolynes, *Science* **254**, 1598 (1991).
89. Y. Mizutani and T. Kitagawa, *Chem. Rec.* **1**, 258 (2001). M. H. Vos, *Biochim. Biophys. Acta* **1777**, 15 (2008).
90. J. E. Straub and M. Karplus, *Chem. Phys.* **158**, 221 (1991). M. Meuwly, O. M. Becker, R. Stote, and M. Karplus, *Biophys. Chem.* **98**, 183 (2002). R. Elber and Q. H. Gibson, *J. Phys. Chem. B* **112**, 6147 (2008).

91. M. R. Armstrong, J. P. Ogilvie, M. L. Cowan, A. M. Nagy, and R. J. D. Miller, *Proc. Natl. Acad. Sci. USA* **100**, 4990 (2003). A. M. Nagy, V. Raicu, and R. J. D. Miller, *Biochim. Biophys. Acta* **1749**, 148 (2005).
92. F. Rosca, A. T. N. Kumar, X. Ye, T. Sjodin, A. A. Demidov, and P. M. Champion, *J. Phys. Chem. A* **104**, 4280 (2000). F. Rosca, A. T. N. Kumar, D. Ionascu, T. Sjodin, A. A. Demidov and P. M. Champion, *J. Chem. Phys.* **114**, 10884 (2001). F. Rosca, A. T. N. Kumar, D. Ionascu, X. Ye, A. A. Demidov, T. Sjodin, D. Wharton, D. Barrick, S. G. Sligar, T. Yonetani, and P. M. Champion, *J. Phys. Chem. A* **106**, 3540 (2002). P. M. Champion, F. Rosca, D. Ionascu, W. Cao, and X. Ye, *Faraday Discuss.* **127**, 123 (2004). F. Gruia, X. Ye, D. Ionascu, M. Kubo, and P. M. Champion, *Biophys. J.* **93**, 4404 (2007). F. Gruia, M. Kubo, X. Ye, D. Lonascu, C. Lu, R. K. Poole, S. Yeh, and P. M. Champion, *J. Am. Chem. Soc.* **130**, 5231 (2008).
93. P. K. Agarwal, S. R. Billeter, P. R. Rajagopalan, S. J. Benkovic, and S. Hammes-Schiffer, *Proc. Natl. Acad. Sci. USA* **301**, 2794 (2002). P. Agarwal, *J. Am. Chem. Soc.* **127**, 15248 (2005). A. Jiménez, P. Clapés, and R. Crehuet, *J. Mol. Model*. **14**, 735 (2008).
94. A. Warshel and W. W. Parson, *Q. Rev. Biophys.* **34**, 563 (2001).
95. J. K. Agbo, D. M. Leitner, D. A. Evans, and D. J. Wales, *J. Chem. Phys.* **123**, 124304 (2005).
96. B. C. Dian, A. Longarte, P. R. Winter, and T. S. Zwier, *J. Chem. Phys.* **120**, 133 (2004).
97. H. Teramoto and T. Komatsuzaki, unpublished.
98. A. Nagy, V. Prokhorenko, and R. J. D. Miller, *Curr. Opin. Struct. Biol.* **16**, 654 (2006).
99. T. S. Zwier, *J. Phys. Chem. A* **110**, 4133–4150 (2006).
100. M. Ikeguchi, J. Ueno, M. Sato, and A. Kidera, *Phys. Rev. Lett.* **94**, 078102 (2005). S. Omori, S. Fuchigami, M. Ikeguchi, and A. Kidera, *J. Chem. Phys.* **132**, 115103 (2010).
101. Y. M. Koyama, T. J. Kobayashi, S. Tomoda, and H. R. Ueda, *Phys. Rev. E* **78**, 046702 (2008).
102. Y. Gao, M. Koyama, S. F. El-Mashtoly, T. Hayashi, K. Harada, Y. Mizutani, and T. Kitagawa, *Chem. Phys. Lett.* **429**, 239 (2006). M. Koyama, S. Neya, and Y. Mizutani, *Chem. Phys. Lett.* **430**, 404 (2006).
103. N. Ota and D. A. Agard, *J. Mol. Biol.* **351**, 345 (2005).
104. S. W. Lockless and R. Ranganathan, *Science* **286**, 295 (1999).
105. K. Sharp and J. J. Skinner, *Proteins* **65**, 347 (2006).
106. T. Ishikura and T. Yamato, *Chem. Phys. Lett.* **432**, 533 (2006).
107. D. M. Leitner, *J. Chem. Phys.* **130**, 195101 (2009).
108. D. Segal, A. Nitzan, and P. Hänggi, *J. Chem. Phys.* **119**, 6840 (2003).
109. M. del Valle, R. Gutierrez-Laliga, C. Tejedor, and G. Cuniberti, *Nat. Nano* **2**, 176 (2007). T. Yuge and A. Shimizu, *J. Phys. Soc. Jpn.* **78**, 083001 (2009).
110. Q. Zhong, A. P. Baronavski, and J. C. Owrutsky, *J. Chem. Phys.* **118**, 7074 (2003).
111. P. Saalfrank, *Chem. Rev.* **106**, 4116 (2006).
112. Y. Togashi and A. S. Mikhailov, *Proc. Natl. Acad. Sci. USA* **104**, 8697–8702 (2007).
113. B. Juanico, Y. H. Sanejouand, F. Piazza, and P. De Los Rios, *Phys. Rev. Lett.* **99**, 238104 (2007).
114. G. Kopidakis, S. Aubry, and G. P. Tsironis, *Phys. Rev. Lett.* **87**, 165501 (2001).